Citation
Aufort, J. and Schuitemaker, A. and Green, R. and Demichelis, R. and Raiteri, P. and Gale, J.D. 2022. Determining the Adsorption Free Energies of Small Organic Molecules and Intrinsic Ions at the Terrace and Steps of Calcite. Crystal Growth and Design. 22 (2): pp. 1445-1458. http://doi.org/10.1021/acs.cgd.1c01414

Determining the adsorption free energies of small organic molecules at terraces and steps of calcite

Julie Aufort[1,2], Alicia Schuitemaker[1], Rebecca Green[1], Raffaella Demichelis[1], Paolo Raiteri[1] and Julian D. Gale[1]

[1]*Curtin Institute for Computation/The Institute for Geoscience Research (TIGeR), School of Molecular and Life Sciences, Curtin University, P.O. Box U1987, Perth, WA 6845, Australia*
[2]*Géosciences Environment Toulouse (GET), Observatoire Midi-Pyrénées, Université de Toulouse, CNRS, IRD, CNES, UPS, 14 Avenue Edouard Belin, Toulouse 31400, France*

Abstract

The adsorption of small molecules containing two different organic functional groups at terrace and step sites on the morphology-dominating $\{10\bar{1}4\}$ surface of calcite at the interface with aqueous solution was studied using free energy methods. Polarizability was taken into account through using a thermodynamically-based force field developed for calcium carbonate using the AMOEBA model that contains static multipoles and self-consistent induced dipoles. The influence of including polarization was examined by comparing to data obtained with a fixed charge rigid-ion model. The strong hydration layers above the basal plane of calcite were shown to hinder the direct attachment of the small species studied, including the constituent ions of the mineral. Only the species bearing an amino group, namely methylammonium and glycine, demonstrated favorable adsorption free energies. The ability of amino groups to more readily pass through the hydration layers than carboxylate and carbonate groups can be explained by their weaker solvation free energies, while the carbonate ions within the calcite surface with which they bind are also less strongly hydrated than calcium ions. Acetate, glycine and methylammonium were all found to be able to directly bind to one growth site at the acute step of calcite. This is at variance with results obtained with a rigid-ion model, in which all binding free energies are endergonic. Thus, including polarization allows for a description of the adsorption process that is more consistent with experimental observations, particularly at calcite steps, and for determination of more reliable atomic scale mechanisms for calcite growth and its modification by organic additives.

1. Introduction

Biomineralization is an organism-driven process involving the selective uptake of aqueous ions from the local environment to form precise functional architectures (1). When

biogenic in origin, the naturally formed material is in fact an organo-mineral composite in which the organic matrix and mineral fraction are closely intertwined from the microscopic to the macroscopic scale, forming highly specific hierarchical structures. The organic substance is mainly composed of lipids, polysaccharides and proteins (2). Along with other processes, such as confinement (3) and local pH regulation (4, 5), the inclusion of soluble organic molecules and macromolecules allows for precise control over the nucleation and growth of the biomineral, resulting in the production of a wide range of crystal sizes, morphologies and compositions with varied functions (e.g. 6, 7, 8). The presence of organic material is indeed known to affect the morphology and polymorphism of the resulting crystal (9,10, 11) and the effect of a specific organic species on the mineral formation is highly dependent on the physico-chemical conditions (12, 13, 14). Among the more than 64 different biomineral phases, either amorphous or crystalline, that have been documented, calcium carbonate $CaCO_3$ is the most abundant (2). It has three anhydrous polymorphs – calcite, aragonite and vaterite. Calcite is the most stable polymorph at ambient conditions and its morphology is dominated by the $\{10\bar{1}4\}$ cleavage plane, which therefore is the most widely studied calcite surface (15). In addition to being important for biomineralization processes, the control of calcite growth by organic molecules is also relevant for the development of new hybrid functional materials (16, 17), the inhibition of scale formation in water systems for industrial applications and cultural heritage preservation (18, 19), the sequestration of CO_2 (20), and the prevention of medical conditions affecting gravity sensors, such as positional vertigo (21). A greater understanding of how organic molecules interact with calcium carbonate is thus relevant to many potential applications.

A large number of experimental studies have explored the effects of organic molecules such as polysaccharides (22, 23), alcohols (24), amino acids and peptides (25, 26, 27, 28) on calcium carbonate nucleation and growth. In particular, the effects of amino acid residues in which sequences of proteins are rich, such as glycine, aspartate and glutamate, have been extensively documented, both as monomers and longer-chain polymers (29, 30, 28, 31). However, the mechanisms by which specific organic functional groups control the growth process remain poorly understood, particularly in regard to the binding of the organic species at the step edges and growth sites, and the competition with constituent ions for adsorption. Indeed, limitations lie in the difficulty to experimentally probe the dynamics of atomic-scale interactions between the mineral surface and the adsorbing organic species.

Computer simulations can help better understand experimental observations and gain insight into the mechanisms involved by providing an atomic scale description of these

processes along with quantitative data such as binding free energies. However, most studies based on molecular dynamics conducted to date have used forces derived from either a rigid-ion model (e.g. 32, 33, 34) or a shell model (35) which proved unsatisfactory for describing liquid water (36). While rigid-ion models can be parametrized to describe the aqueous phase and the bulk mineral well, achieving transferability between the two is more difficult. Recently, Raiteri et al. (37) developed a polarizable force field based on the AMOEBA model for calcium carbonate and its interactions with water. It was successfully applied to the solid phase and found to compare well with experiment and DFT in describing the calcite $\{10\bar{1}4\}$ – water interface (38). In this work, we use classical molecular dynamics (MD) based on this polarizable force field to investigate the interactions of carboxylate and ammonium functional groups with calcite, by studying the adsorption of acetate, methylammonium and zwitterionic glycine, along with the constituent ions, calcium, and carbonate, onto the basal plane and steps of the $\{10\bar{1}4\}$ surface of calcite. In order to elucidate the effect of polarization we also perform MD simulations with an AMOEBA based force field that was developed and characterized in our previous work (39). Implications for calcite growth inhibition or promotion by organic additives will be discussed, as well as the effect of accounting for polarization in the modelling of adsorption processes.

2. Methods

2.1. Force fields

All simulations were performed using classical molecular dynamics (MD) based on force fields. Fixed charge models, when fitted carefully against structural properties and relevant thermodynamic quantities, such as solvation free energies, can provide an accurate description of ions in solution at reasonably low computational cost (40). However, they do not account for many-body effects, such as electronic polarization, which makes the description of heterogeneous chemical systems more challenging. Processes at the mineral-water interface, such as adsorption on a crystalline surface, require the adsorbate to progress from an aqueous environment with a high dielectric constant to a bound state with a crystalline material characterized by a low dielectric constant and stronger ionic interactions. Although it comes at a higher computational cost, including polarizability should improve the transferability between the aqueous phase and the crystalline state, and is expected to provide a more robust description of the adsorption process. For these reasons, in this work we have used the polarizable force field that was recently developed for calcium carbonate in water based on the AMOEBA model (37). Additionally, the force field developed by Raiteri et al. (41) for calcium

carbonate systems in conjunction with the flexible simple point charge water model (SPC/Fw) by Wu et al. (42) was used for comparison with a fixed charge rigid-ion model.

All MD simulations conducted with the polarizable AMOEBA force field were performed with the OpenMM code (43) and run on GPUs using mixed precision (44, 45) with the inclusion of the PLUMED plug-in (46, 47). Simulations were run at 300 K in the NVT ensemble after an equilibration run for 100 ps in the NPT ensemble and with a 1 fs time step. The temperature was controlled by a Langevin thermostat with a friction coefficient of 1 ps^{-1}.

For the rigid-ion force field, all MD simulations were performed using the LAMMPS code (48) again in conjunction with the PLUMED library. Simulations were run using a 1 fs time step in the NVT ensemble after equilibration of the simulation cell along the direction perpendicular to the calcite surface. The temperature was maintained at 300 K by a Nosé-Hoover thermostat with a relaxation time of 0.1 ps.

2.2. Adsorption on the basal plane of calcite

The aqueous $\{10\bar{1}4\}$ terrace of calcite was modelled using a 50 x 50 x 85 $Å^3$ 3D periodic cell, which consisted of an approximately 35 Å thick calcite slab (1,440 $CaCO_3$ formula units) repeating in the *xy* plane covered by a layer of water of about 50 Å (3,914 water molecules). The full system was composed of this calcite-water interface and one adsorbate species. The adsorbate was either a small molecule containing at least one organic functional group (ammonium and/or carboxylate) or a constituent ion of the mineral.

The thermodynamics of adsorption on the calcite $\{10\bar{1}4\}$ flat surface was determined using well-tempered (49) multiple walker (50) metadynamics (51). The binding free energy profiles were constructed using two collective variables in order to bias the distance to the surface and accelerate water exchange. The distance between the adsorbate and the surface was taken as the projection along *z* (i.e. the surface normal) of the distance between the position of Ca, C, or N as appropriate to the adsorbing species and an appropriate Ca or C atom located below the adsorption site, but in the middle of the calcite slab (a Ca or C atom from the interfacial layer was not chosen to avoid the risk of pulling this ion out of the surface). The water coordination number at a given adsorption site on the calcite surface was described using the switching function;

$$CN = \sum_i \frac{1 - \left(\frac{r_i - d_0}{r_0}\right)^n}{1 - \left(\frac{r_i - d_0}{r_0}\right)^m}$$

where r_i is the distance between the ion and the oxygen of the ith water molecule. The parameters were chosen so that the function would overlap with the first peak of the pair distribution function with the water oxygen, i.e., n = 6, m = 12, d_0 = 1.8 Å (Ca^{2+}) and 0.8 Å (CO_3^{2-}), r_0 =1.0 Å (Ca^{2+}) and 3 Å (CO_3^{2-}) for all the simulations run with AMOEBA. With the rigid-ion force field, the coordination number of calcium was systematically biased regardless of the adsorbing species and the chosen parameters were n = 4, m = 10, d_0 = 2.1 Å, r_0 =1.0 Å.

Metadynamics simulations were run with 16 or 30 independent walkers for the AMOEBA and rigid-ion forcefields, respectively, with a bias factor of 5 in both cases. Gaussians were laid every 1 ps with a height of k_BT and width of 0.1 Å for the distance and 0.1 for the coordination number. Aggregate simulation times of about 300 ns were performed for each adsorption free energy calculation to ensure well-converged sampling. A cylindrical harmonic restraining wall with a spring constant of 10,000 kJ/mol nm^{-2} was implemented parallel to *z* to ensure the adsorbate remained laterally confined near the surface site of interest. An additional harmonic wall restraining the adsorbing ion to stay within 15 Å from the calcite surface along *z* was used to limit the space explored given that the free energy reaches a plateau well before this point; the same spring constant of 10,000 kJ/mol nm^{-2} was used.

2.3. Adsorption at calcite steps

The $\{10\bar{1}4\}$ calcite-water interface built for the AMOEBA and rigid-ion simulations of the adsorption processes at the steps was modelled through a monoclinic unit cell with lattice parameters of 51.6 Å, 51.6 Å, 58.1 Å, 90°, 90°, 101.9° which contains 1,216 $CaCO_3$ formula units and 2,600 water molecules. Both the calcite and water layers were approximately 30 Å thick. As described in De La Pierre et al. (34), half of the uppermost calcite layer was removed to create periodic acute and obtuse steps separated by equal amounts of upper and lower terrace. The steps ran parallel to the [100] crystallographic direction of the above monoclinic cell. In total, the system has sixteen potential binding sites immediately adjacent to the steps; eight different sites at both the acute and obtuse steps, due to four symmetry inequivalent positions along each step with the possibility of binding at the top and bottom of the step edge (Figure 1). There are numerous further terrace sites as a function of the distance from the step edge that may differ slightly from the two ideal terrace sites corresponding to being above Ca^{2+} or CO_3^{2-}, but examination of this large number of possible configurations is beyond the scope of the present work.

The free energy of adsorption at the step edges was computed using a similar protocol to the metadynamics calculations performed for the flat surface. In all cases we used the *z* component of the distance between the Ca, C and N of the adsorbing species to a Ca or C underneath the adsorption site, which was located in the middle of the slab. The adsorption site was defined as a calcium or carbonate ion at the step edge. In the case of glycine two free energy calculations were performed, one for the adsorption of the NH_3^+ terminus and one for the carboxylate terminus. For the adsorption of the negatively-charged species and functional groups, we also used the coordination number of the Ca on the lower terrace that was closest to the adsorption site as a second collective variable. For all these calculations, the cylindrical restraint was replaced with an elliptical one, which had a short axis of 3 Å parallel to the step edge and a long axis of 4 Å normal to the step edge (i.e. this corresponds to maximum region widths of 6 and 8 Å, respectively). This restraint shape was chosen to allow the adsorbate to explore a wider region of space on the upper and lower terraces, without being able to reach the adjacent adsorption site. The harmonic restraining spring constant remained unchanged. A restraining wall was then used to limit the adsorbing ion to stay within 15 Å from the calcite surface along *z*. As per the adsorption on the calcite flat $\{10\bar{1}4\}$ surface, the free energy profiles were obtained using well-tempered multiple walker metadynamics with all parameters kept the same excepted for the bias factor which was increased from 5 to 10 for the adsorption of carboxylate and carbonate groups. For the adsorption of acetate and the carboxylate group of glycine at site 1 on the acute step (Figure 1), we noticed that during the metadynamics simulations the walkers were not able to freely cross the adsorption free energy barrier, which is normally an indication that an important (slow) degree of freedom has been missed. Hence, we repeated the simulations using one extra collective variable that allowed us to describe the orientation of the adsorbate relative to the step edge. To achieve this, we used the cosine of the angle of the C-C and C-N bond vector and the [101] lattice vector, which allows us to discriminate between all the possible orientations of the adsorbate at the step edge. However, because of the use of one extra collective variable the metadynamics simulations are much slower to converge and we decided to limit the exploration of the *z* collective variable to 5 Å from the surface. The projection of the free energy along the z axis can then be generated for the full range of distances by connecting the curves computed with 2 and 3 CVs at a height were there was no longer a preferential orientation of the adsorbate.

3. Results and Discussion

3.1. Adsorption free energies on the basal plane of calcite

The adsorption of the constituent ions of calcite, and of several molecules bearing carboxylate ($-CO_2^-$) and/or (protonated) amino ($-NH_3^+$) functional groups, was first investigated on the terraces of the defect-free $\{10\bar{1}4\}$ surface.

The 2D free energy maps as a function of the adsorbate-surface distance and water coordination number for the AMOEBA force field are given in Figure 2. All free energy plots show a monotonous profile upon reduction of the distance between the adsorbate and the calcite surface until the adsorbing ion or molecule comes into contact with the hydration layers at a distance of ~4 Å. The interaction between a calcium ion and the second water layer on the surface is accompanied by a decrease in its coordination number from ~7 to ~6. For all negatively charged adsorbates, the coordination number of the calcium ion by water at the adsorbing terrace site decreases from 1 to 0 when forming the contact bound state. These maps confirm that biasing the water coordination number of calcium as the adsorbing site is essential in obtaining accurate energetics for the adsorption process, as shown by the high activation free energy to reach the surface adsorbed state, and is consistent with the slow water exchange rate of ~4 ns calculated at the surface which is more than ten-times slower than that of calcium in bulk solution (38). In contrast, the adsorption of amino groups does not require a significant variation of the water coordination number of the carbonate group at the surface. With a shorter residence time of water on surface carbonates of ~1 ns, increasing water exchange at these sites through application of an explicit bias is not as crucial as for the adsorption on calcium surface sites. Therefore, for the adsorption of cations, including calcium, at the step edges we did not use the coordination number collective variable to improve the convergence of the 1D free energy profile as this was unnecessary.

The 1D adsorption free energy profiles calculated with the AMOEBA and rigid-ion force fields, obtained by integrating out the water coordination number, are shown in Figure 3 and the corresponding adsorption free energies, taken as the energy difference between the minimum and the free ion in solution, are listed in Table 1. In order to adsorb onto the flat surface of calcite, negatively-charged species must replace the water molecules located directly above calcium sites that form the first hydration layer, whereas the cations are expected to substitute for water molecules located above carbonate groups in the second hydration layer (Figure 4). All the adsorption free energy profiles of negatively- and positively-charged species obtained with the AMOEBA force field reveal a repulsive potential associated with replacing a water molecule in the first hydration layer, whose position is taken to be at 2.19 Å from the

surface (38), indicating that these species are unable to penetrate the first hydration layer. In contrast, a free energy minimum can be found for each species in the region of the second hydration layer around 3.33 Å (38). The adsorption free energies of the positively-charged species in the second hydration layer are all exergonic relative to the free cation in solution, with -8.5, -4.7 and -4.6 kJ/mol for calcium, glycine N-terminus and methylammonium, respectively. However, while the substitution of the amino groups for water in the second hydration layer only requires a moderate energy barrier of about 7-8 kJ/mol to be overcome, calcium substitution for water is accompanied by a more significant barrier of about 19 kJ/mol. For the negatively-charged species, the binding free energies of carbonate and acetate, +7.0 and +4.8 kJ/mol, respectively, are both endergonic relative to the free anions in solution, whereas the binding free energy of the glycine C-terminus is slightly negative, though is comparable to thermal fluctuations at ambient conditions (-1.4 kJ/mol). The configuration corresponding to the stable free energy minimum on the free energy profile of glycine N-terminus at 3.4 Å is identical to that found in the free energy profile of the C-terminus at 4.8 Å (with the difference in height being due to the N-C distance) and is shown in Figure 4. Overall, direct binding to the surface is not favorable for any of the species studied and significant indirect binding via a solvent-shared state is achieved only by positively-charged species, i.e. calcium and amino groups.

Similar trends are observed in the 1D free energy profiles calculated for the organic species using the rigid-ion force field, with none of the species being able to bind directly to the surface. The profiles for the acetate and glycine C-terminus present significantly higher energy barriers (more than 30 kJ/mol) to reach less stable minima in the region of the second hydration layer. The energy barrier to substitute for water molecules in the second water layer is significantly lower for amino groups (about 10 kJ/mol), although the resulting adsorption free energies relative to the free species in solution are positive, with +7.1 and +9.3 kJ/mol for methylammonium and glycine, respectively, and correspond to shallow minima. However, the constituent ions of calcite, calcium and carbonate, show free energy profiles with the rigid-ion model that are significantly different from those determined with the polarizable force field. While the AMOEBA model predicts a thermodynamically favorable substitution of calcium for water in the second hydration layer, the rigid-ion model not only found that this process led to a highly endergonic binding free energy, +27.3 kJ/mol, but also that the configuration corresponds to something more akin to an inflexion point in the free energy profile rather than a significant minimum. Unlike the carboxylate group of glycine, which is essentially unable to penetrate the hydration layers (adsorption free energy of +51.4 kJ/mol), carbonate ions meet

with the least resistance when crossing the hydration layers. In contrast to the other species, the adsorption free energy profile of carbonate not only shows a stable minimum (-2.5 kJ/mol) in the region of the second water layer at 3.4 Å, but also in the first water layer at 2.7 Å, although the latter is shallow (~1 kJ/mol deep) and corresponds to a positive adsorption free energy of +3.5 kJ/mol, relative to the energy of the free ion in solution. Despite differences in the free energy profile of carbonate between polarizable and non-polarizable force fields, a similar conclusion can be drawn that direct binding of carbonate ions onto the $\{10\bar{1}4\}$ plane surface of calcite is unfavorable. Overall, all species are found to be unable to substitute efficiently for water molecules in the hydration layers and present exclusively positive binding free energies with the exception of carbonate, for which solvent-shared binding is exergonic, but only to an extent that is of the order of ambient thermal fluctuations. Compared to AMOEBA, most adsorption free energies are shifted toward more endergonic values with the rigid-ion force field, which is consistent with the changes in the polarization as species transition from solution to interact with the surface.

Both the force fields with and without polarizability show that the strong hydration of the $\{10\bar{1}4\}$ plane is responsible for the weak binding of constituent ions and small organic molecules on the surface. This has also been reported in several other studies. For instance, Kerisit and Parker (52) calculated adsorption free energy profiles of calcium and other metal ions using classical molecular dynamics with a shell model force field, and found that calcium could not penetrate the first hydration layer due to highly repulsive electrostatic interactions with the water layer. Furthermore, Magdans et al. (53) used grazing incidence X-ray diffraction and classical MD to show that glycine preferentially substitutes for water molecules in the second hydration layer instead of binding directly to the surface. Similarly, Nada (33) found via classical MD that aspartic acid, another molecule bearing both amino and carboxylate organic functional groups, could not directly bind to the calcite $\{10\bar{1}4\}$ surface.

The trend we observed with both force fields that amino groups seem to approach the surface more easily than carboxylate groups was also reported by Aschauer et al. (54) who, using a shell model force field, calculated more exergonic adsorption free energies for polyaspartic acid than polyacrylic acid owing to the presence of nitrogen on its backbone. The fact that carbonate groups, to which amino groups preferentially bind, are less strongly hydrated than calcium ions could account for the smaller energy barriers amino groups are faced with when approaching the surface. Furthermore, amino group-containing species have less exergonic solvation free energies compared to carboxylate-bearing molecules (-264 kJ/mol

for methylammonium vs. -330 kJ/mol for acetate (39)) and thus interact less strongly with their hydration shell. This makes the case of glycine, containing both an amino and carboxylate group, particularly interesting. While its N-terminus is able to indirectly bind to the terraces with an exergonic adsorption free energy, the penalty for dehydration of is too high for the C-terminus to cross through the hydration layers. At neutral pH, glycine is a zwitterion but in acidic and alkaline conditions it behaves either as a glycinium cation or a glycinate anion, respectively. While the effect of glycine on the growth rate of calcite is moderate (28), this amino acid has been shown to alter crystal morphologies and exert control on polymorph selection (25, 55, 27, 56). In particular, glycine's ability to stabilize vaterite over calcite was attributed by Shivkumara et al. (57) to its bifunctional nature.

3.2. Adsorption free energies at the obtuse and acute steps of calcite

Crystallization processes on mineral surfaces, such as adsorption or dissolution, occur preferentially at sites associated with structural inhomogeneities such as defects, dislocations, steps and kinks. The $\{10\bar{1}4\}$ surface of calcite shows two non-equivalent step orientations, one forming an acute angle with the basal plane, and the other an obtuse angle (Figure 4). We thus explored the adsorption of the constituent ions and organic molecules at both the acute and obtuse steps of calcite $\{10\bar{1}4\}$. Binding energies corresponding to the most significant minima and obtained from the 1D projection are reported in Table 2. Given that in some cases, particularly when two free energy basins overlap along the coordination number coordinate, the projection along the distance collective variable may not reflect properly the barrier heights, which could lead to an underestimation of the adsorption free energies, the binding energies obtained from the minimum energy path of the 3D free energy profiles are also reported in Table S1 along with the full list of all free energy minima. Distances to the surface are given relative to the upper layer of calcium ions. A distance of $\sim$0 Å from the surface thus indicates that the adsorption occurs directly on the lower terrace next to the step whereas a height of $\sim$2 Å points to adsorption at the edge of the upper terrace. The same notation as that introduced in De La Pierre et al. (34) was used to identify the symmetry non-equivalent adsorption sites (Figure 1).

3.2.1 Adsorption of constituent ions

Adsorption free energy profiles of the constituent ions of calcite, calcium and carbonate, obtained with the polarizable force field are shown in Figure 5. Adsorption of calcium ions is not favorable at the obtuse steps, nor at position B of the acute step, with either

positive adsorption free energies being obtained or negative ones that are only of the order of ambient thermal energy. However, the symmetry non-equivalent site (position A) on the acute step appears to provide more favorable binding sites, with more significant binding energies of -13.8 and -11.0 kJ/mol at the lower and upper terraces, respectively. This is at variance with both current (this work) and previous (34) results obtained with the rigid-ion force field that only found positive adsorption free energies for Ca^{2+} and particularly unfavorable binding on the lower terraces, where the natural growth site is expected. However, a high energy barrier of ~16 kJ/mol has to be overcome in the AMOEBA simulations in order to reach the natural 'growth site' on the lower terrace. This indicates that even though stable minima are identified on the lower terrace by the polarizable force field, direct migration to the growth site remains kinetically limited as suggested by De La Pierre et al. (34). A similar conclusion can be drawn for carbonate ions as the adsorption free energies on the lower terrace are positive for all four adsorption sites. Significantly stable minima, corresponding to adsorption free energies of -20.5 and -10.5 kJ/mol, were only found on the upper terrace sites of the obtuse step, at positions 1 and 2, respectively. In contrast, results obtained from the rigid-ion force field show that thermodynamically favorable binding can occur at all upper terrace sites, with the most exergonic adsorption free energy (-20.8 kJ/mol) corresponding to position 1 on the acute step.

Results obtained with the polarizable force field challenge some of the findings related to the calcite growth mechanism proposed by De La Pierre et al. (34) from classical MD based on the rigid-ion model. In particular, the finding that calcium ions can only adsorb after carbonate can be questioned in light of the new data from the AMOEBA calculation. While carbonate is faced with essentially no energy barrier to adsorb at the obtuse upper step edge, the same is also true for calcium at the acute step, though the trend in the relative strength of adsorption still remains valid. Although both calcium and carbonate are now found to adsorb at clean steps, because the ions only bind at the acute or obtuse step, respectively, the formation of ion pairs will be necessary to add the oppositely charged species at that step, as previously found for the rigid-ion model. As carbonate again prefers to bind at the upper step edge with AMOEBA, it appears likely that occupation of the site at the lower step edge that is commensurate with the underlying crystal structure will only occur following ion pair formation, though further work is required to verify this. The difference between calcium and carbonate in terms of choice of preferred step edge with the AMOEBA model also appears to be consistent with the observed rates of single-ion growth determined experimentally (58, 59).

3.2.2 Adsorption of carboxylate groups

For simulations conducted with a given force field, the 1D adsorption free energy profiles of the two molecules bearing carboxylate functions, namely acetate and glycine, show similar trends (Figure 6; note the full 2D free energy maps are given in Figures S1 and S2). Results obtained using the AMOEBA model indicate that adsorption of acetate and glycine on the lower terraces of both obtuse and acute steps is characterized by exclusively positive values of the free energy, except for position 1 on the acute step where glycine binds exergonically, although with a free energy of the order of ambient thermal energy (-2.1 kJ/mol). Instead, both acetate and glycine C-terminus adsorb preferentially on the upper terrace at position 2 of the obtuse step, with adsorption free energies of -8.5 and -10.4 kJ/mol, respectively. From these configurations, shown in Figure 7e for acetate and Figure 7f for glycine, high energy barriers of ∼29 and ∼23 kJ/mol, respectively, must be traversed for the molecules to transition from the upper to the lower terrace.

The case of the adsorption at position 1 on the acute step is notably different from that of the other possible binding sites. As mentioned in the methods section, the use of a third collective variable describing the orientation of the adsorbate relative to the step was required to achieve accurate sampling of the configuration space. The 1D profile showed that glycine could transition more easily from the upper to the lower terrace of the acute step at position 1, with a barrier height of ∼27 kJ/mol compared to ∼38 kJ/mol for acetate. The 2D maps of the free energy as a function of the distance to the surface and the orientation of the adsorbate shown in Figure 8 can provide more information on the mechanisms involved. First, they confirm that a significantly higher energy barrier is required for acetate (∼50 kJ/mol) to transition from the upper to the lower terrace compared to glycine (∼33 kJ/mol). They also reveal that, for both acetate and glycine, there are in reality two possible configurations associated with a free energy minimum on the lower terrace and that the free energy barrier for acetate to transition between the two states (∼22 kJ/mol) is twice that of glycine (∼11 kJ/mol). In the case of acetate, the two minima are about 9 kJ/mol less stable than the configuration in which acetate is bound to the upper terrace. In contrast, the minimum free energy path for glycine to move from the upper to the lower terrace involves first reaching a configuration on the lower terrace that is about 5 kJ/mol less stable than when the molecule is bound to the upper terrace, followed by moving to a second configuration that is equally as stable as the upper terrace state.

The different configurations corresponding to free energy minima at position 1 of the acute step are all shown as inserts on Figures 9 and 10, representing the 3D maps of the free

energy as a function of the distance to the surface, the coordination number of the adsorption site and the orientation of the adsorbate, for acetate and glycine, respectively. Acetate is found to adsorb on the lower terrace either with its C-C bond oriented nearly perpendicular to the surface (i.e. tilted by only 20° from the [101] direction), or with its C-C bond aligned with the direction of step propagation. For glycine, only configurations in which the C-N bond is oriented nearly parallel to the step correspond to free energy minima on the lower terrace, and the two minima differ by the orientation of the amino group, which points to either extreme of the [110] step direction.

Overall, similar trends are found with the AMOEBA force field for both molecules bearing a carboxylate group, but glycine is altogether more strongly bound to the surface, regardless of whether this to the upper or lower terrace sites. Glycine can also transition more easily from the upper terrace to the adsorption site on the lower terrace of the acute step, to which it binds more strongly than acetate.

The bifunctional nature of glycine could account in part for its stronger binding ability to the calcite steps than acetate, as observed with the polarizable force field. As discussed in the earlier section on the calcite terraces, amino groups interact less strongly with water than carboxylate groups due to their less hydrophilic character. Compared to acetate, the presence of an amino group at the other extremity of the molecule could help glycine cross through the hydration layers more easily and facilitate its approach to the growth site. Furthermore, the amino group could also contribute to stabilizing glycine once it has reached the binding site. Indeed, contrary to acetate, glycine is not linear and the molecule is bent at the level of the aliphatic carbon with a $\widehat{NCC}$ angle of about 107°. As a result, the amino group remains at the level of the upper terrace when the carboxylate group is bound to the lower terrace and is thus able to interact with the adjacent carbonate groups. In particular, in the case of the configuration shown in the bottom right insert of Figure 10, two hydrogen atoms are found to be at a distance of ~1.9 Å and ~2.5 Å from the oxygen of the adjacent carbonate groups at the upper and lower terraces, respectively (Figure S3). It is possible that hydrogen bonds between hydrogen atoms of the amino group and carbonate oxygens could stabilize the two configurations of glycine adsorbed on the lower terrace relative to that of acetate and lead to less endergonic binding energies.

Two factors could explain the preference of both acetate and glycine for one specific binding site at the acute step (i.e., position 1); the geometry of that particular site and/or possible differences in water exchange rates relative to the other binding sites. For instance,

the trends in water exchange rates calculated with the rigid-ion force field were found to be significantly different between the obtuse step, at which an alternating sequence of fast and slow waters was observed, and the acute step at which water exchange was uniformly slow, suggesting different kinetics of ion adsorption (60). While the wider angle between the lower and upper terraces at the obtuse step could limit the possibility of stabilizing interactions with the adjacent carbonate groups compared to the acute step, it is more difficult to understand why binding at position 1 of the acute step is more favorable than at the adjacent site, at position 2. Survival functions for the water molecules around positions 1 and 2 of the obtuse and acute steps are shown in Figure S4. Slower water exchange is found for position 1 at the acute step, with a residence time of 6.1 ns, whereas the fastest exchange is observed at site 2 of the obtuse step with a residence time of 0.7 ns. While a longer residence time explains the relatively high energy barrier found at site 1 of the acute step, it is also indicative of a stronger interaction between calcium and water, which subsequently results in greater binding between this calcium site and the adsorbing molecule. In any case, these findings are consistent with the experimental observation that adding glycine to a solution in which calcite is being grown affects the morphology of the acute steps but not that of the obtuse steps (25).

In contrast to the above results, when polarizability is not included in the simulations, acetate and glycine are unable to bind at any of the expected potential growth sites for nucleation of a new row of the step edge on calcite. The free energy profiles (Figure 6) and maps (Figure S2) for acetate and glycine obtained with the rigid-ion model show that both acetate and glycine are met with a repulsive potential when approaching the step edges. Free energy minima are only found for acetate at position 1 of the acute step on both the lower and upper terraces, but they both correspond to significantly endergonic binding free energies relative to the free species in solution. As per the flat surface, simulations carried out with the non-polarizable force field predict an unfavorable binding of acetate and glycine onto the calcite steps. This is inconsistent with the competitive adsorption of molecules other than constituent ions at the growth sites as the reason commonly provided for calcite growth modification by organics in experimental studies (e.g. 25, 19, 28) unless the thermodynamic trends at kink sites turn out to be radically different. For instance, the mechanism proposed by et Gan al. (61) to explain glycine's ability to stabilize vaterite over calcite in an alkaline silica gel involves the inhibition of calcite growth by adsorption of the molecule at the calcite growth site. Contrary to the conclusions drawn from simulations carried out with the rigid-ion force field, our results obtained with the polarizable force field show that it is possible for glycine to bind directly to one of the lattice sites adjacent to the step and lower terrace with an exergonic

binding free energy, although this is only of the order of ambient thermal energy. This is consistent with the proposed mechanism, although the magnitude of the binding would suggest it is a reversible process. Even though calcite grows primarily by screw dislocations, sufficient binding of glycine at the step would eventually block the propagation of the kink and inhibit growth.

3.2.3 Adsorption of amino groups

The 1D adsorption free energy profiles of the two molecules bearing amino functional groups, namely methylammonium and glycine, are shown in Figure 11. The simulations conducted using AMOEBA reveal that methylammonium adsorbs preferentially via solvent-shared binding at 3.4 Å from the surface (e.g. Fig. 7g), although the adsorption free energies, ranging from -1.0 to -4.0 kJ/mol, are mostly within ambient thermal fluctuations (Table S2). From this state, the molecule is able to adsorb directly onto position A of the upper terrace at the acute step (Fig. 7i) by crossing a low energy barrier of about 3 kJ/mol. A minimum of the same depth, -0.5 kJ/mol, can then be reached on the lower terrace but requires crossing a ~6 kJ/mol energy barrier. All other minima correspond to endergonic adsorption free energies. Similarly, the AMOEBA adsorption free energy profiles of glycine on calcite steps show thermodynamically favorable solvent-shared binding at about 3.4 Å from the surface, with the free energies ranging from -2.4 to -4.0 kJ/mol. However, a more exergonic binding site was found on the lower terrace at position A on the acute step, with an adsorption free energy of -13.0 kJ/mol. Overall, glycine can access a more stable lattice site adjacent to the acute step on the lower terrace (position A) and reach this more easily than methylammonium as the energy barrier is about half the magnitude.

Comparison with simulations carried out with the rigid-ion force field shows that, as for carboxylate groups, binding of methylammonium and glycine through its N-terminus on calcite steps is thermodynamically unfavorable when polarization is not accounted for. None of the adsorption sites located at the acute step, whether the ones corresponding to continuation of the crystal lattice immediately adjacent to the step, or to the step edge of the upper terrace, are associated with free energy minima. Shallow free energy minima are only found at the obtuse step, and they all correspond to endergonic values relative to the free molecule in solution. Note that positions further away from the steps were not explored with either force field owing to their higher computational cost, therefore the possibility of more favorable direct binding sites than the expected growth sites for nucleation of a new row cannot be excluded, though it would be surprising if these sites differed substantially from those on the terraces.

Direct comparison between calculated binding free energies and values obtained by fitting adsorption isotherms is not straightforward, as experimental datasets describe a macroscopic phenomenon encompassing multiple individual reactions. However, the average binding free energies calculated here for glycine (+6.7 and -1.7 kJ/mol for C-terminus and N-terminus, respectively) at the lattice sites adjacent to the step and the lower terrace are comparable to that of calcium (-1.4 kJ/mol), where the relative values are in agreement with the findings of Montanari et al. (28) who measured adsorption free energies ranging from -20 to -25 kJ/mol for glycine and concluded it could compete with calcium for adsorption after comparison to the -28.3 kJ/mol adsorption free energy for calcium measured by Huang et al. (62). Compared to calcium, the average binding free energy of acetate, +11.3 kJ/mol, is significantly weaker. This was also observed by Dobberschutz et al. (63) who reported a 17.4 kJ/mol difference between the two adsorption free energies obtained using a microkinetic model to fit data resulting from growth inhibition experiments. However, the authors calculated similar adsorption free energies for calcium and carbonate, -18.5 and -19.1 kJ/mol respectively, which is at variance with our results showing carbonate as the species with the weakest average binding free energy at the lattice sites adjacent to the step and the lower terrace (+15.7 kJ/mol). In addition to our results pertaining to adsorption at steps rather than kinks, this discrepancy is also likely related to the assumptions made in the microkinetic model whereby the macroscopic growth rate and fitted adsorption free energy would reflect that of the growing step with the weakest inhibition, illustrating the difficulty to reconcile quantities calculated from atomic scale simulations with macroscopic measurements.

4. Conclusions

Including polarizability is found to significantly improve the description of the adsorption process by classical molecular dynamics simulations. While for the terraces, the binding free energies are simply more endergonic in the absence of polarization, discrepancies between the polarizable and non-polarizable force fields are more pronounced in the case of adsorption at calcite steps. With the rigid-ion model, direct binding of the organic molecules, acetate, methylammonium and glycine, was found to be unfavorable at all the lattice sites adjacent to the step and the lower terrace, with either no free energy minima or exclusively endergonic binding free energies relative to the free species in solution. In contrast, all three molecules showed exergonic binding free energies at least one of the growth sites with the AMOEBA model. These findings are more consistent with the experimental observations that calcite growth can be inhibited or slowed down in the presence of such molecules in solution,

along with the commonly proposed mechanism of competitive adsorption of organics over constituent ions at the growth sites. Quantitatively, we find that in the situations where adsorption of organic functional groups is favorable, the binding is only of the order of a few k_BT at best. While this may be at odds with some previous theoretical estimates that are significantly exothermic, often based on extracting only internal energies of adsorption with incomplete sampling of competing hydration, we believe that the present modest binding free energies are more reasonable. Experimentally, peptides are usually more effective as growth modification than individual amino acids and there is a variation with the number of residues, all of which suggests the need for multiple functional groups to achieve significant adsorption strength. Furthermore, in the context of biomineralization, adsorption of organics often needs to be reversible to avoid stoichiometric incorporation.

Of course, it is important to note here that the primary growth sites will be at kinks, whereby a given step edge row will be propagated. Here the results are more relevant to the nucleation of a new additional row at a step edge, which is required for propagation across the terrace, though given the common occurrence of screw dislocations at the calcite surface this nucleation barrier can often be avoided. While the study of the 16 possible kink sites is challenging and beyond the scope of this study, it is likely that similar trends may occur for these positions as for the step edges. This calls for further work on the binding of ions and organic molecules at all possible kink sites that also takes into account polarizability in order to gain a full picture of calcite growth processes at the atomic scale. The high computational cost associated with using the currently available polarizable force field means such simulations will have to rely on the increasing availability and performance of GPUs and/or the development of exascale computing.

Acknowledgment

This research was funded by the Australian Research Council (ARC DP16100677, FT1810038, FL180100087) and Curtin University. This work was supported by computing resources provided by the Pawsey Supercomputing Centre and the National Computational Infrastructure.

References

1. Mann S. (Ed.) Biomineralization: Principles and concepts in bioinorganic materials chemistry Oxford University Press, New York **2001**, p. 1

2. Weiner, S.; Dove, P. An Overview of Biomineralization Processes and the Problem of the Vital Effect. *Reviews in Mineralogy and Geochemistry* **2003**, *54*(1), 1-29. DOI: 10.2113/0540001

3. Stephens, C.J.; Ladden, S.F.; Meldrum, F.C.; Christenson, H.K. Amorphous calcium carbonate is stabilized in confinement. *Advanced Functional Materials* **2010**, *20*(13), 2108-2115. DOI: 10.1002/adfm.201000248

4. Frankel, R.B.; Bazylinski, D.A. Biologically induced mineralization by bacteria. *Reviews in Mineralogy and Geochemistry* **2003**, *54*(1), 95-114. DOI: 10.2113/0540095

5. Kamennaya, N.A.; Ajo-Franklin, C.M.; Northen, T.; Jansson, C. Cyanobacteria as biocatalysts for carbonate mineralization. *Minerals* **2012**, *2*(4), 338-364. DOI: 10.3390/min2040338

6. Hincke, M.T.; Gautron, J.; Panheleux, M.; Garcia-Ruiz, J.; Mc Kee, M.D.; Nys, Y. Identification and localization of lysozyme as a component of shell membranes and eggshell matrix. *Matrix Biology* **2000**, *19*(5), 443-453. DOI: 10.1016/S0945-053X(00)00095-0

7. Wilt, F.H. Biomineralization of the spicules of sea urchin embryos. *Zoological Science* **2002**, *19*(3), 253-261. DOI: 10.2108/zsj.19.253

8. Aizenberg, J.; Tkachenko, A.; Weiner, S.; Addadi, L.; Gendler, G. Calcitic microlenses as part of the photoreceptor system in brittlestars. *Nature* **2001**, *412*, 819-822. DOI: 10.1038/35090573

9. Falini, G.; Albeck, S.; Weiner, S.; Addadi, L. Control of aragonite or calcite polymorphism by mollusk shell macromolecules. *Science* **1996**, *271*(5245), 67-69. DOI: 10.1126/science.271.5245.67

10. Gebauer, D.; Colfen, H.; Verch, A.; Antonietti, M. The multiple roles of additives in CaCO3 crystallization: A quantitative case study. *Adv. Mater.* **2009**, *21*(4), 435-439. DOI: 10.1002/adma.200801614

11. Verch, A.; Gebauer, D.; Antonietti, M.; Colfen, H. How to control the scaling of CaCO3: a “fingerprinting techniaue to classify additives. *Phys. Chem. Chem. Phys.* **2011**, *13*(37), 16811-16820. DOI: 10.1039/c1cp21328h

12. Dutour Sikiric, M.; Furedi-Milhofer, H. The influence of surface-active molecules on the crystallization of biominerals in solution. *Advances in Colloid and Interface Science*, **2006**, *128-130*, 135-158. DOI: 10.1016/j.cis.2006.11.022

13. Hou, W.; Feng, Q. Morphology and formation mechanism of vaterite particles grown in glycine-containing aqueous solutions. *Materials Science & Engineering C*, **2006**, *26*(4), 644-647. DOI: 10.1016/j.msec.2005.09.098

14. Gower, L.B. Biomimetic model systems for investigating the amorphous precursor pathway and its role in biomineralization. *Chemical Reviews* **2008**, *108*(11), 4551-4627. DOI: 10.1021/cr800443h

15. Ruiz-Agudo, E.; Putnis, C.V. Direct observations of mineral fluid reactions using atomic force microscopy: the specific example of calcite. *Mineralogical magazine* **2012**, *76*(1), 227-253. DOI: 10.1180/minmag.2012.076.1.227

16. Sommerdijk, N.A. J. M.; de With, G. Biomimetic $CaCO_3$ mineralization using designer molecules and interfaces. *Chem. Rev.* **2008**, *108*(11), 4499-4550. DOI: 10.1021/cr078259o

17. Kato, T.; Sakamoto, T.; Tatsuya, N. Macromolecular templating for the formation of inorganic-organic hybrid structures. *MRS Bull* **2010**, *35*(2), 127-132. DOI: 10.1557/mrs2010.632

18. Chaussemier, M.; Pourmohtasham, E.; Gelus, D.; Pecoul, N.; Perrot, H.; Ledion, J.; Cheap-Charpentier, H.; Horner, O. State of the art of natural inhibitors of calcium carbonate scaling. A review article. *Desalination* **2015**, *356*, 47-55. DOI: 10.1016/j.desal.2014.10.014

19. Rodriguez-Navarro, C.; Benning, L.G. Control of crystal nucleation and growth by additives. *Elements* **2013**, *9*(3), 203-209. DOI: 10.2113/gselements.9.3.203

20. Matter, J.M.; Kelemen, P.B. Permanemt storage of carbon dioxide in geological reservoirs by mineral carbonation. *Nature Geoscience* **2009**, *2*, 837-841. DOI: 10.1038/ngeo683

21. Rose-Martel, M.; Sliley, S.; Hincke, M.T. Novel identification of matrix proteins involved in calcitic biomineralization. *J. Proteomics* **2015**, *116*, 81-96. DOI: 10.1016/j.jprot.2015.01.002

22. Yang, M.; Stipp, S.L.S., Harding J. Biological control on calcite crystallization by polysaccharides. *Crystal Growth & Design* **2008**, *8*(11), 4066-4074. DOI: 10.1021/cg800508t

23. Nielsen, J.W.; Sand, K. K.; Pedersen, C.S.; Lakshtanov, L.Z.; Winther, J. R.; Willemoes, M.; Stipp, S.L.S. Polysaccharide effects on calcite growth: The influence of composition and branching. *Crystal Growth & Design* **2012**, *12*(10), 4906-4910. DOI: 10.1021/cg300772h

24. Sand, K.K.; Yang, M.; Makovicky, E.; Cooke, D.J.; Hassenkam, T.; Bechgaard, K.; Stipp, S.L.S. Binding of ethanol on calcite: the role of the OH bond and its relevance to biomineralization. *Langmuir* **2010**, *26*(19), 15239-15247. DOI: 10.1021/la101136j

25. Orme, C.A.; Noy, A.; Wierzbicki, A.; McBride, M.T.; Grantham, M.; Teng, H.H.; Dove, P.M.; DeYoreo, J.J. Formation of chiral morphologies through selective binding of amino acids to calcite surface steps. *Nature* **2001**, *411*, 775-779. DOI: 10.1038/35081034

26. Wu C., Wang X., Zhao K., Cao M., Xu H., Xia D., Lu J.R. Molecular modulation of calcite dissolution by organic acids. *Crystal Growth & Design* **2011**, *11*(7), 3153-3162. DOI: 10.1021/cg200403t

27. Tobler, D.J.; Rodriguez-Blanco, J.D.; Dideriksen, K.; Sand, K.K.; Bovet, N.; Benning, L.G.; Stipp, S.L.S. The effect of aspartic acid and glycine on amorphous calcium carbonate (ACC) structure, stability and crystallization. *Procedia Earth and Planetary Science* **2014**, 10, 143-148. DOI: 10.1016/j.proeps.2014.08.047

28. Montanari, G.; Lakshtanov, L.Z.; Tobler, D.J.; Dideriksen, K.; Dalby, K.N.; Bovet, N.; Stipp, S.L.S. Effect of aspartic acid and glycine on calcite growth. *Crystal Growth & Design* **2016**, *16*(9), 4813-4821. DOI: 10.1021/acs.cgd.5b01635

29. Elhadj, S.; Salter, E.A.; Wierzbicki, A.; De Yoreo, J.J.; Han, N.; Dove, P.M. Peptide controls on calcite mineralization: Polyaspartate chain length affects growth kinetics and acts as a stereochemical switch on morphology. *Crystal Growth & Design* **2006**, *6*(1), 197-201. DOI: 10.1021/cg050288+

30. Njegic-Dzakula, B.; Brecevic, L.; Falini, G.; Krajl, D. Calcite crystal growth kinetics in the presence of charged synthetic polypeptides. *Crystal Growth & Design* **2009**, *9*(5), 2425-2434. DOI: 10.1021/cg801338b

31. Stepic, R.; Jurkovic, L.; Klementyeva, K.; Ukrainczyk, M.; Gredicak, M.; Smith, D.M.; Krajl, D.; Smith, A.-S. Adsorption of aspartate derivatives to calcite surfaces in aqueous

environment. *Crystal Growth & Design* **2020**, *20*(5), 2853-2859. DOI: 10.1021/acs.cgd.0c00061

32. Freeman, C.L.; Asteriadis, I.; Yang, M.; Harding, J.H. Interactions of organic molecules with calcite and magnesite surfaces. *J. Phys. Chem. C.* **2009**, *113*(9), 3666-3673. DOI: 10.1021/jp807051u

33. Nada, H. Difference in the conformation and dynamics of aspartic acid on the flat regions, step edges, and kinks of a calcite surface: a molecular dynamics study. *J. Phys. Chem. C* **2014**, *118*(26), 14335-14345. DOI: 10.1021/jp502332c

34. De La Pierre, M.; Raiteri, P.; Stack, A.G.; Gale J.D. Uncovering the atomistic mechanism for calcite step growth. *Angew. Chem. Int. Ed.* **2017**, *56*(29), 8464-8467. DOI: 10.1002/anie.201701701

35. De Leeuw, N.H.; Cooper, T.G. A computer modelling study of the inhibiting effect of organic adsorbates on calcite crystal growth. *Crystal Growth & Design* **2004**, *4*(1), 123-133. DOI: 10.1021/cg0341003

36. Van Maaren, P.; van der Spoel, D. Molecular dynamics simulations of water with novel shell-model potentials. *Journal of Physical Chemistry B* **2001**, *105*(13), 2618-2626. DOI: 10.1021/jp003843l

37. Raiteri, P.; Schuitemaker, A.; Gale, J.D. Ion pairing and multiple ion binding in calcium carbonate solutions based on a polarizable AMOEBA force field and ab initio molecular dynamics. *The Journal of Physical Chemistry B* **2020**, *124*(17), 3568-3582. DOI: 10.1021/acs.jpcb.0c01582

38. Brugman S., Raiteri P., Accordini P., Megens F., Gale J., Vlieg E. The calcite (104) surface – electrolyte structure: a 3D comparison of surface X-ray diffraction and simulations. *J. Phys. Chem. C* **2020**, *124*(34), 18564-18575. DOI: 10.1021/acs.jpcc.0c04094

39. Schuitemaker, A.; Aufort, J.; Koziara, K.B.; Demichelis, R.; Raiteri, P.; Gale, J.D. Simulating the binding of organic functional groups to aqueous calcium carbonate species. *Phys. Chem. Chem. Phys.* **2021**

40. Raiteri, P.; Demichelis, R.; Gale, J. D. Development of Accurate Force Fields for the Simulation of Biomineralization. *Methods Enzymol.* **2013**, *532*, 3−23. DOI: 10.1016/B978-0-12-416617-2.00001-1

41. Raiteri, P.; Demichelis, R.; Gale, J. D. Thermodynamically Consistent Force Field for Molecular Dynamics Simulations of Alkaline-Earth Carbonates and Their Aqueous Speciation. *J. Phys. Chem. C* **2015**, *119*(43), 24447−24458. DOI: 10.1021/acs.jpcc.5b07532

42. Wu, Y.; Tepper, H.; Voth, G. A. Flexible Simple Point-charge Water Model With Improved Liquid-state Properties. *J. Chem. Phys.* **2006**, *124*(2), 024503/1-12. DOI: 10.1063/1.2136877

43. Eastman, P.; Swails, J.; Chodera, J. D.; McGibbon, R. T.; Zhao, Y.; Beauchamp, K. A.; Wang, L.-P.; Simmonett, A. C.; Harrigan, M. P.; Stern, C. D.; et al. OpenMM 7: Rapid development of high-performance algorithms for molecular dynamics. *PLoS Comput. Biol.* **2017**, *13*(7), e1005659-17. DOI: 10.1371/journal.pcbi.1005659

44. Friedrichs, M. S.; Eastman, P.; Vaidyanathan, V.; Houston, M.; Legrand, S.; Beberg, A. L.; Ensign, D. L.; Bruns, C. M.; Pande, V. S. Accelerating molecular dynamic simulation on graphics processing units. *J. Comput. Chem.* **2009**, *30*(6), 864−872. DOI: 10.1002/jcc.21209

45. Eastman, P.; Pande, V. S. Efficient nonbonded interactions for molecular dynamics on a graphics processing unit. *J. Comput. Chem.* **2010**, *31*(6), 1268-1272. DOI: 10.1002/jcc.21413

46. The PLUMED consortium. Promoting transparency and reproducibility in enhanced molecular simulations. *Nature Methods* **2019**, *16*(8), 670–673. DOI: 10.1038/s41592-019-0506-8

47. Tribello, G. A.; Bonomi, M.; Branduardi, D.; Camilloni, C.; Bussi, G. PLUMED 2: New Feathers for an Old Bird. *Comput. Phys. Commun.* **2014**, *185*(2), 604–613. DOI: 10.1016/j.cpc.2013.09.018

48. Plimpton, S. Fast parallel algorithms for short-range molecular dynamics. *J. Comput. Phys.* **1995**, *117*(1), 1−19. DOI: 10.1006/jcph.1995.1039

49. Barducci, A.; Bussi, G.; Parrinello, M. Well-Tempered Metadynamics: A Smoothly Converging and Tunable Free-Energy Method. *Phys. Rev. Lett.* **2008**, *100*(2), 020603. DOI: 10.1103/PhysRevLett.100.020603

50. Raiteri, P.; Laio, A.; Gervasio, F. L.; Micheletti, C.; Parrinello, M. Efficient Reconstruction of Complex Free Energy Landscapes by Multiple Walkers Metadynamics. *J. Phys. Chem. B* **2006**, *110*(8), 3533– 3539, DOI: 10.1021/jp054359r

51. Laio, A.; Parrinello, M. Escaping free-energy minima. *Proc. Natl. Acad. Sci. U. S. A.* **2002**, *99*(20), 12562–12566. DOI: 10.1073/pnas.202427399

52. Kerisit, S.; Parker, S.C. Free energy of adsorption of water and metal ions on the $\{10\bar{1}4\}$ calcite surface. *Journal of the American Chemical Society* **2004**, *126*(32), 10152-10161. DOI: 10.1021/ja0487776

53. Magdans, U.; Torrelles, X.; Angermund, K.; Gies, H.; Rius, J. Crystalline order of a water/glycine film coadsorbed on the (104) calcite surface. *Langmuir* **2007**, *23*(9), 4999-5004. DOI: 10.1021/la0636659

54. Aschauer, U.; Spagnoli, D.; Bowen, P.; Parker, S.C. Growth modification of seeded calcite using carboxylic acids: atomistic simulations. *Journal of Colloid and Interface Science* **2010**, *346*(1), 226-231. DOI: 0.1016/j.jcis.2010.02.057

55. Ren, D.; Feng, Q.; Bourrat, X. Effects of additives and templates on calcium carbonate mineralization in vitro. *Micron* **2011**, *42*(3), 228-245. DOI: 10.1016/j.micron.2010.09.005

56. Lai, Y.; Chen, L.; Bao, W.; Ren, Y.; Gao, Y.; Yin, Y.; Zhao, Y. Glycine-mediated, selective preparation of monodisperse spherical vaterite calcium carbonate in various reaction systems. *Crystal Growth & Design* **2015**, *15*(3), 1194-1200. DOI: 10.1021/cg5015847

57. Shivkumara, C.; Singh, P.; Gupta, A.; Hegde, M.S. Synthesis of vaterite CaCO3 by direct precipitation using glycine and L-alanine as directing agents. *Materials Research Bulletin* **2006**, *41*(8), 1455-1460. DOI: 10.1016/j.materresbull.2006.01.026

58. Stack, A.G.; Grantham, M.C. Growth rate of calcite steps as a function of aqueous calcium-to-carbonate ratio: Independent attachment and detachment of calcium and carbonate ions. *Crystal Growth & Design* **2010**, *10*(3), 1409-1413. DOI: 10.1021/cg901395z

59. Sand, K.K.; Tobler, D.J.; Dobberschutz, Larsen, K.K.; Makovicky, E.; Andersson, M.P.; Wolther, M.; Stipp, S.L.S. Calcite growth kinetics: dependence on saturation index, Ca2+:CO32- activity ratio and surface atomic structure. *Crystal Growth & Design* **2016**, *16*(7), 3602-3612. DOI: 10.1021/acs.cgd.5b01792

60. De La Pierre, M.; Raiteri, P.; Gale, J.D. Structure and dynamics of water at step edges on the calcite {10-14} surface. *Crystal Growth & Design* **2016**, *16*(10), 5907-5914. DOI: 10.1021/acs.cgd.6b00957

61. Gan, X.; He, K.; Qian, B.; Deng, Q.; Lu, L.; Wang, Y. The effect of glycine on the growth of calcium carbonate in alkaline silica gel. *Journal of Crystal Growth* **2017**, *458*, 60-65. DOI: 10.1016/j.jcrysgro.2016.11.027

62. Huang, Y.C.; Fowkes, F.M.; Lloyd, T.B.; Sanders, N.D. Adsorption of calcium ions from calcium chloride solutions onto calcium carbonate particles. *Langmuir* **1991**, 7(8), 1742-1748. DOI: 10.1021/la00056a028

63. Dobberschutz, S.; Nielsen, M.R.; Sand, K.K.; Civioc, R.; Bovet, N.; Stipp, S.L.S. Andersson M.P. The mechanisms of crystal growth inhibition by organic and inorganic inhibitors. *Nature Communications* **2018**, *9*, 1578-1584. DOI: 10.1038/s41467-018-04022-0

64. Heberling, F.; Klacik, T.; Raiteri, P.; Gale, J.D.; Eng, P.J.; Stubbs, J.E.; Gil-Diaz, T.; Begovic, T.; Lutzenkirchen, J. Structure and Surface Complexation at the Calcite(104)–Water Interface. *Environ Sci Technol* **2021**, *55*(18), 12403–12413. DOI: 10.1021/acs.est.1c03578

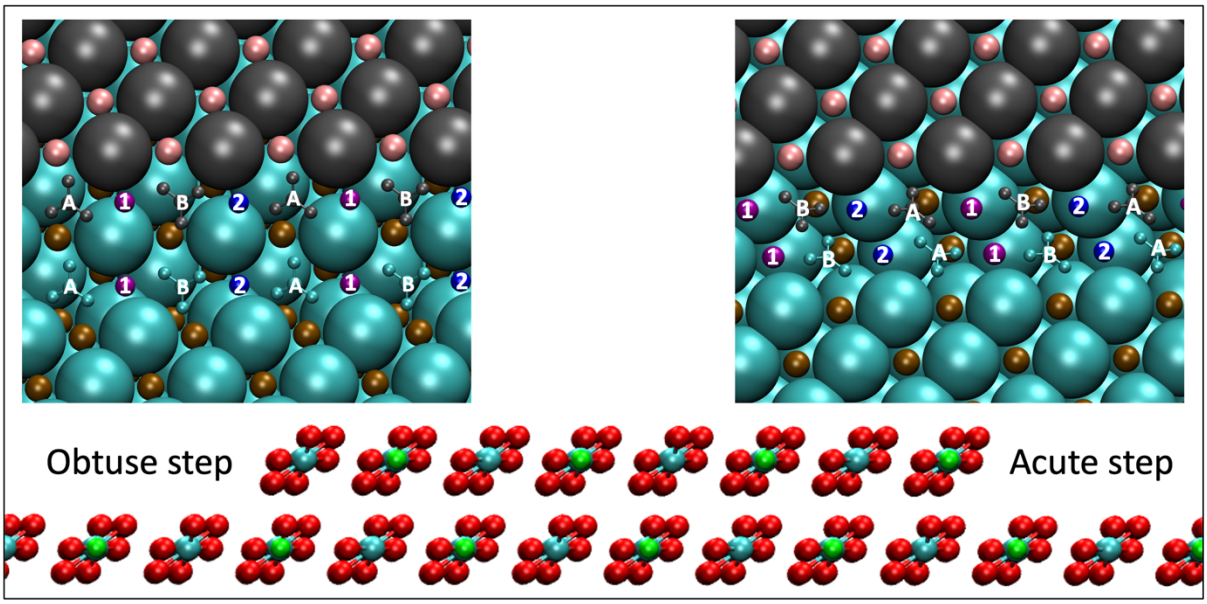

Figure 1. Side view of the obtuse (left) and acute (right) steps on top of the $\{10\bar{1}4\}$ surface of calcite (lower panel), with images taken orthogonal to the step edge (upper panel) where the calcium and carbonate ions are represented as small and large spheres (brown and cyan for lower terrace and pink and gray for the upper terrace), respectively, away from the step edge with only the sites at the step being shown in ball and stick representation (calcium in green, oxygen in red, carbon in cyan). Labels are given for the sites along the step edge to indicate the symmetry unique sites.

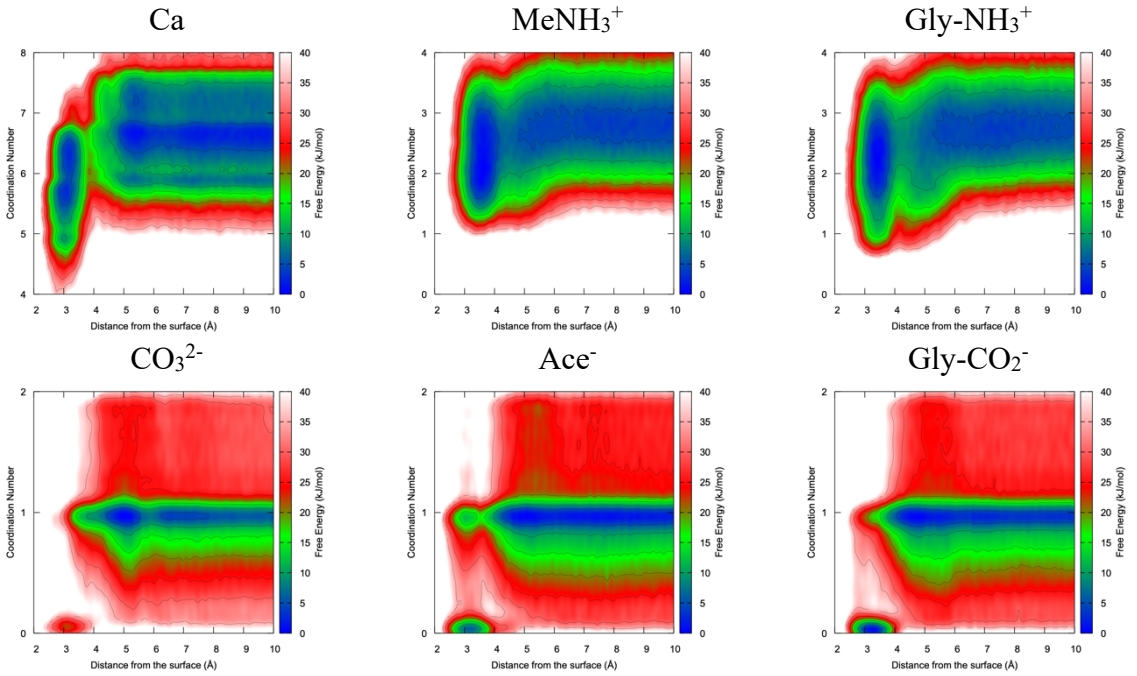

Figure 2. Adsorption free energies for calcium, carbonate, methyl ammonium, acetate and zwitterionic glycine (for both functional groups) as a function of the distance to the calcite surface and of the water coordination number obtained from simulations run with the AMOEBA force field. The free energy landscapes are color coded according to the scale bars on the right-hand side of each panel. For the adsorption of calcium, the coordination number refers to the coordination number of the adsorbate, while in all other cases the coordination number of the adsorption site was used as a second collective variable.

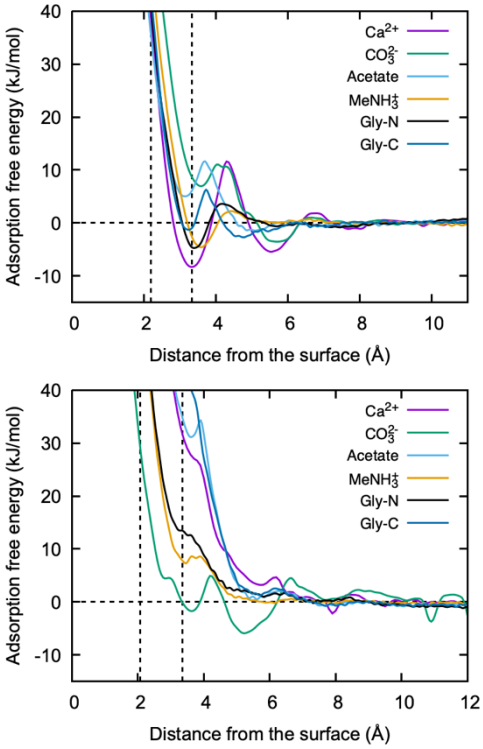

Figure 3. Adsorption free energy profiles as a function of the distance above the surface of calcium (purple), carbonate (green), acetate (blue), glycine C-terminus (light blue), glycine N-terminus (black) and methylammonium (orange) on the $\{10\bar{1}4\}$ terrace of calcite obtained using the AMOEBA (top) and rigid-ion (bottom) force fields. Curves are aligned to $\Delta G = 0$ in the long-range limit. The location of the first two water layers (38) are indicated by vertical dashed lines. The adsorption free energies for calcium and carbonate are taken from Heberling et al. (64).

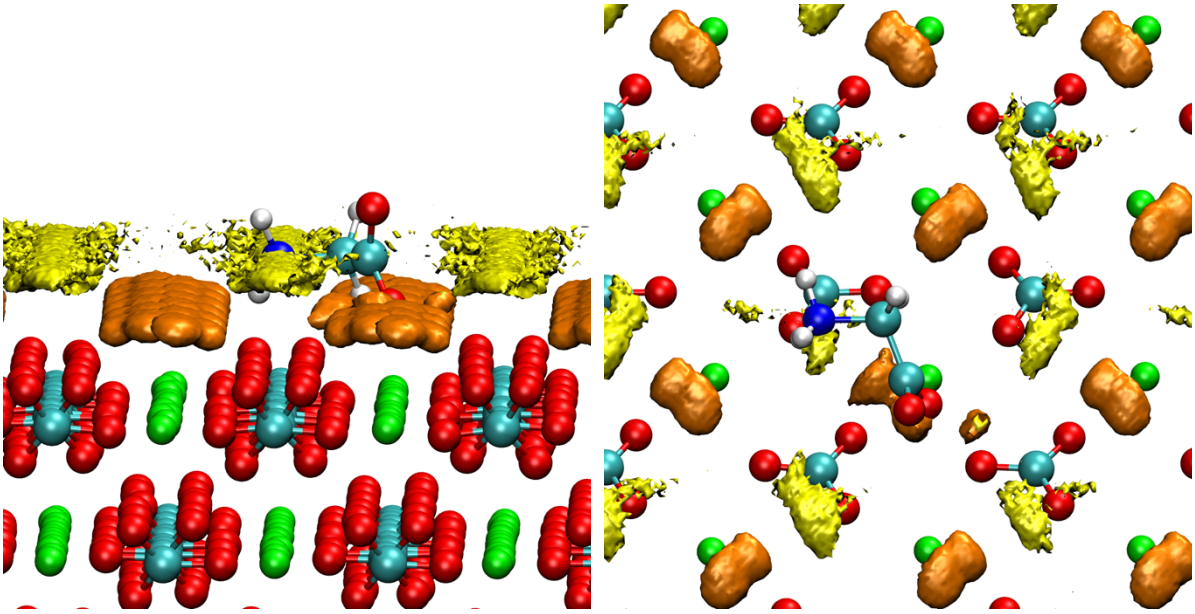

Figure 4. Side (left) and top (right) views of the calcite $\{10\bar{1}4\}$ interfacial structure showing the iso-density surfaces for the oxygen atoms of the water molecules in the first (orange) and second (yellow) hydration layers, and the minimum energy configuration for glycine adsorbed onto the terrace. Calcium in green, oxygen in red, carbon in cyan, hydrogen in white, nitrogen in blue.

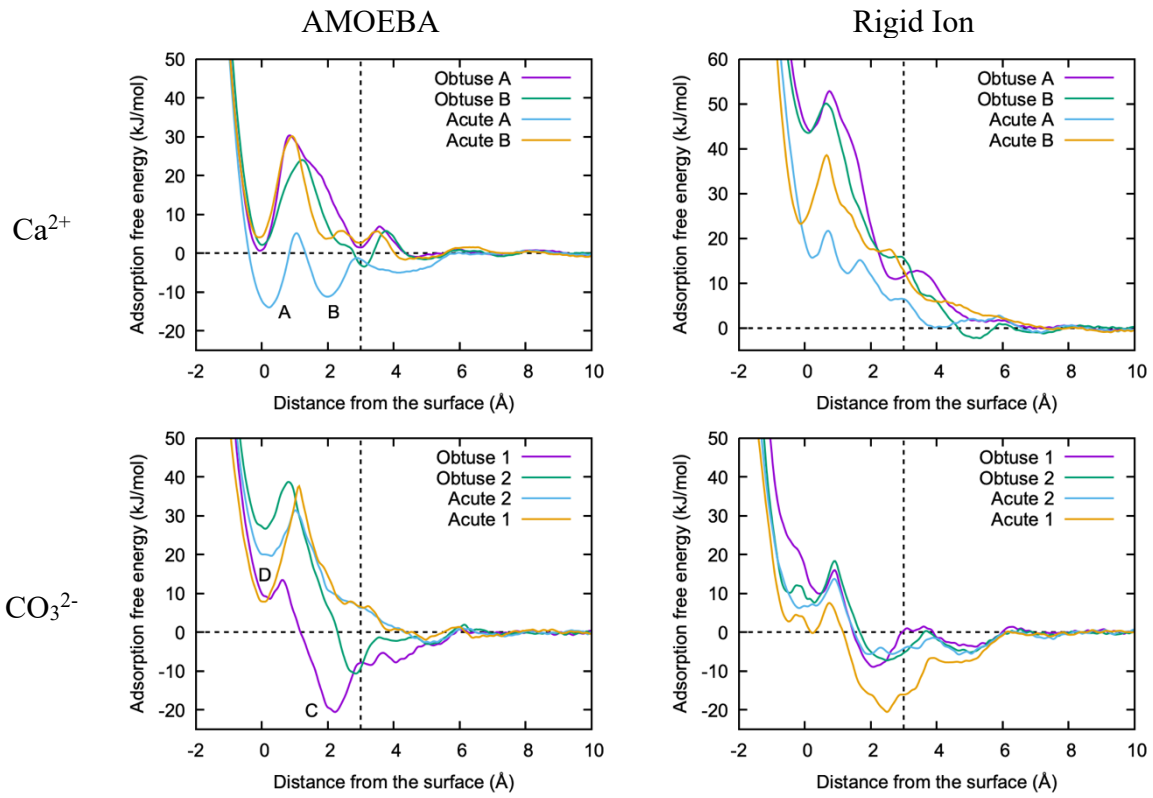

Figure 5. Adsorption free energy profiles obtained with the AMOEBA (left) and rigid-ion force (right) fields of calcium (top) and carbonate (bottom) on the acute and obtuse steps of calcite. The dashed vertical line indicates the approximate position of the upper terrace. Letters adjacent to minima correspond to the atomic configurations shown in Figure 7.

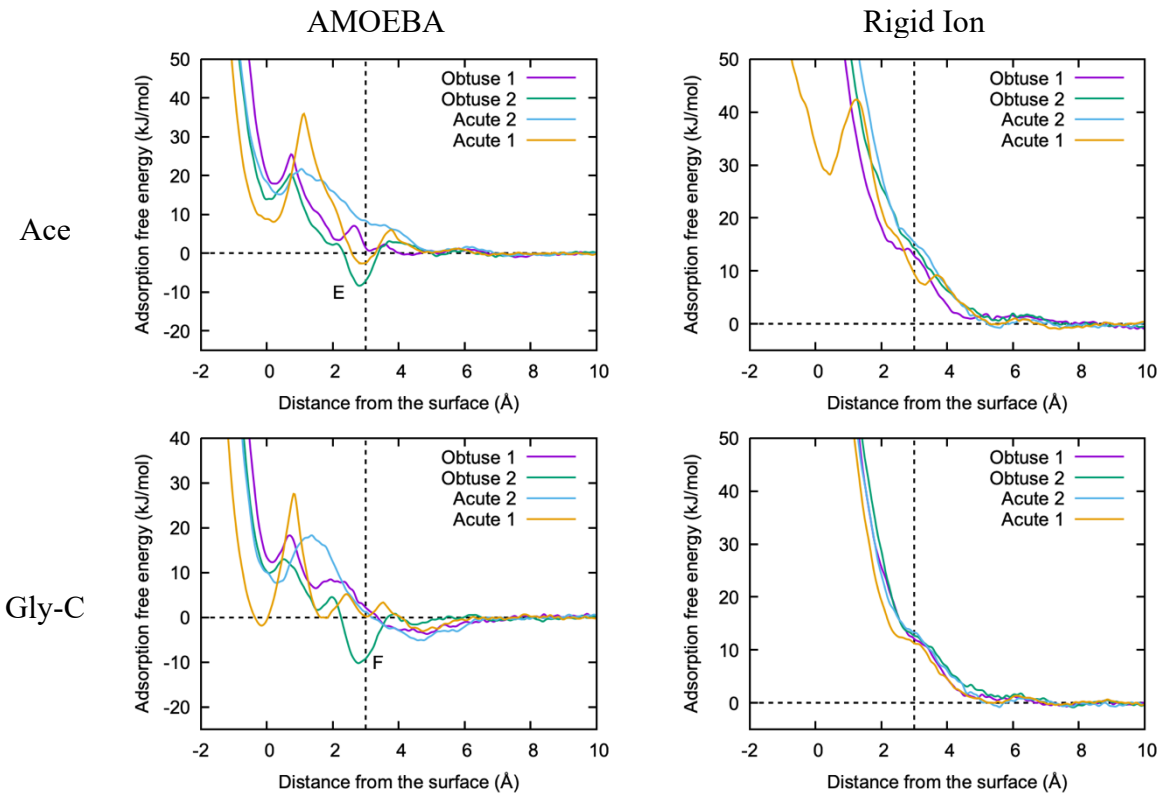

Figure 6. Adsorption free energy profiles obtained with the AMOEBA (left) and rigid-ion (right) force fields for acetate (top) and glycine C-terminus (bottom) on the acute and obtuse steps of calcite. The dashed vertical line indicates the approximate position of the upper terrace. Letters adjacent to minima correspond to the atomic configurations shown in Figure 7.

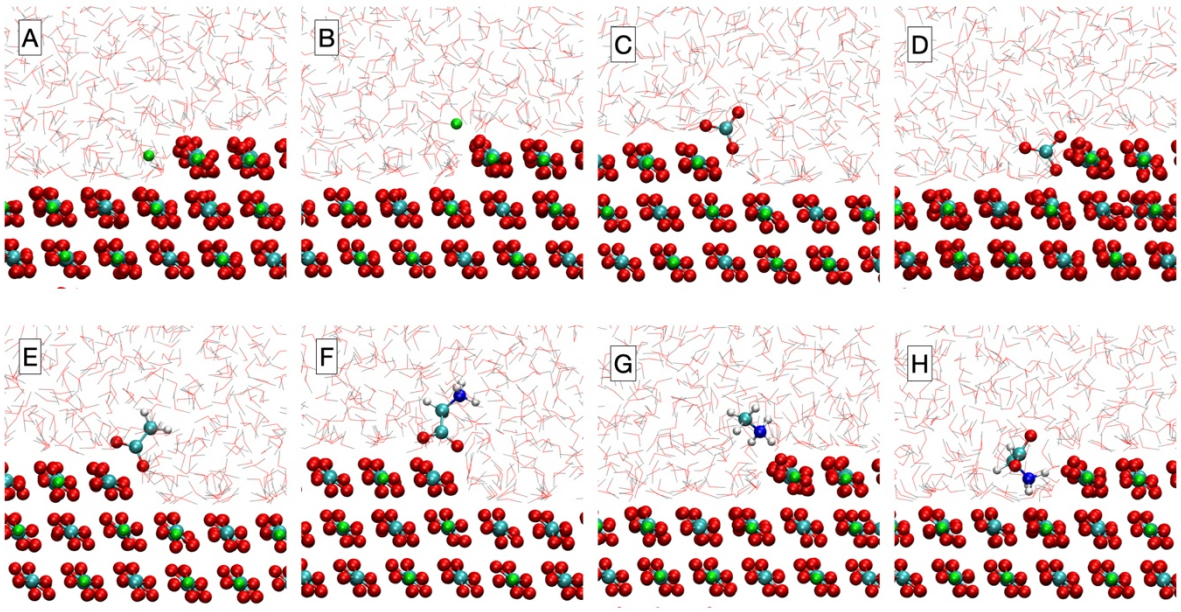

Figure 7. Selected configurations corresponding to the most significant energy minima calculated with the AMOEBA polarizable force field for adsorption onto calcite steps. The letters on the images refer to the free energy minima with the corresponding labels in Figures 5, 6 and 11. Calcium atoms are shown in green, oxygen in red, carbon in cyan, hydrogen in white, nitrogen in blue. The water molecules are represented as thin lines with gray hydrogen atoms to allow the adsorbate to clearly seen.

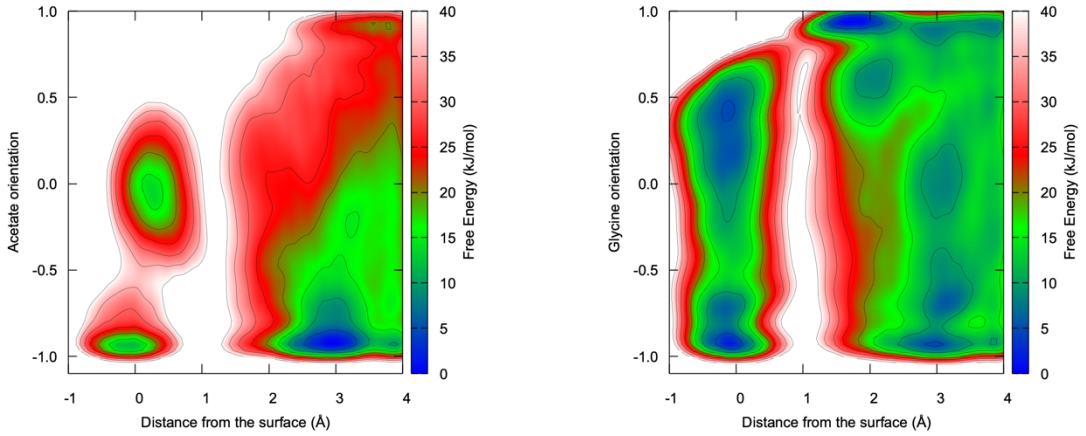

Figure 8. Adsorption free energy maps obtained with the AMOEBA force field for acetate (left) and glycine C-terminus (right) on the acute steps of calcite (site 1) as a function of the vertical distance of the adsorbate from a Ca atom on the lower terrace and of the orientation of the adsorbate with respect to the [101] crystallographic direction (see text for more details).

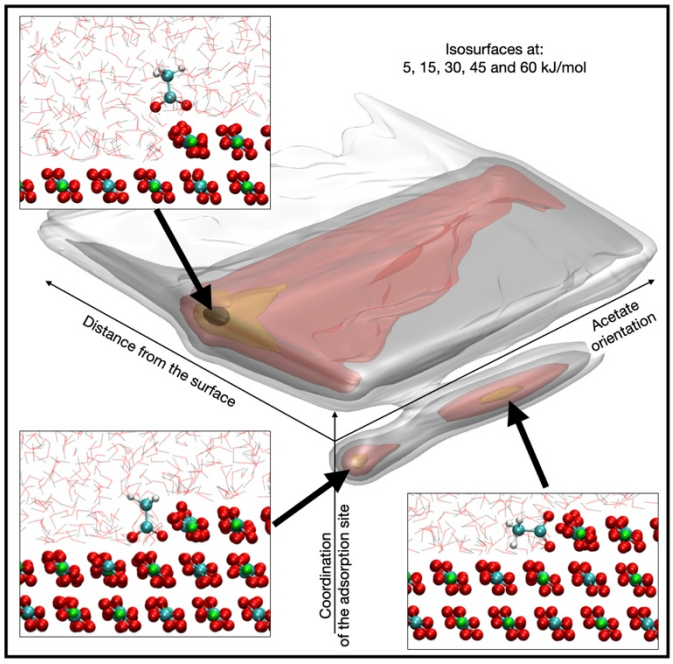

Figure 9. 3D adsorption free energy surface of acetate at the acute step (site 1) obtained with the AMOEBA force field. The insets show typical atomic configurations observed in the main free energy minima. The free energy iso-surfaces were at 5, 15, 30, 45 and 60 kJ/mol from the global minimum and colored in black, orange, red, gray and white, respectively.

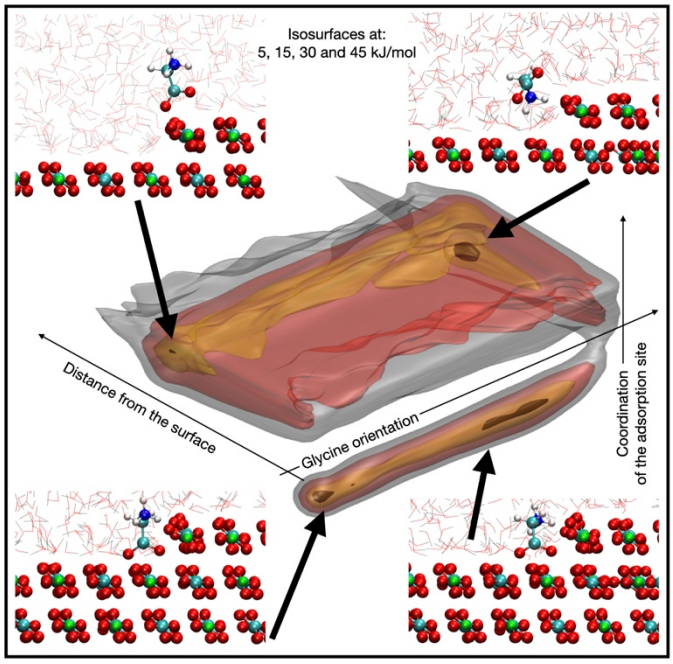

Figure 10. 3D adsorption free energy surface of glycine-CO_2^- terminus at the acute step (site 1) obtained with the AMOEBA force field. The insets show typical atomic configurations observed in the main free energy minima. The free energy iso-surfaces were at 5, 15, 30 and 45 kJ/mol from the global minimum and colored in black, orange, red and gray, respectively.

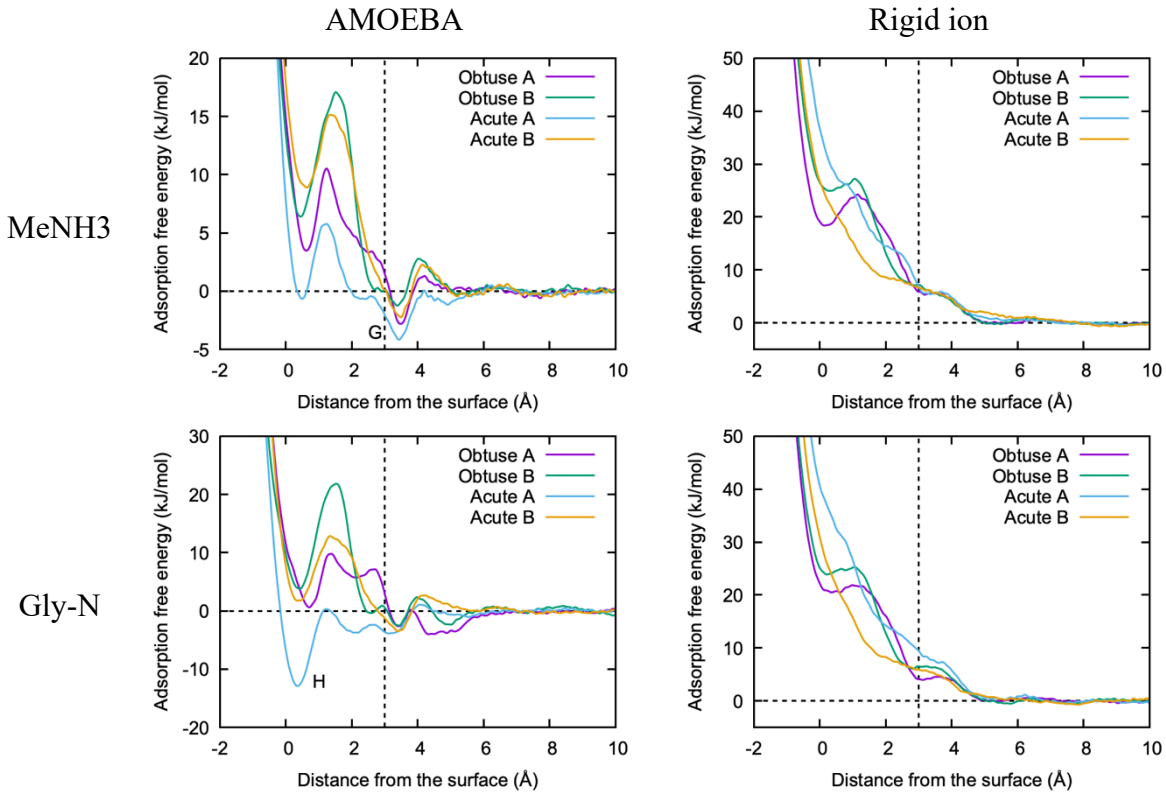

Figure 11. Adsorption free energy profiles obtained with the AMOEBA (left) and rigid-ion (right) force fields of methylammonium (top) and glycine N-terminus (bottom) on the acute and obtuse steps of calcite. The dashed vertical line indicates the approximate position of the upper terrace. Letters adjacent to minima correspond to the atomic configurations shown in Figure 7.

Table 1 Adsorption free energies (kJ/mol) of acetate, glycine, methylammonium, carbonate and calcium on the $\{10\bar{1}4\}$ surface of calcite relative to bulk solution. Distances between the adsorbing species and the surface are given relative to the first layer of calcium ions. Only the energy minima in the region of the second hydration layer (HL2) and from the 1D profiles are reported, except for carbonate where the values are also provided for the first hydration layer (HL1) in the case of the rigid-ion model. The full list of all minima both from 1D profiles and from the minimum energy paths of the 2D profiles can be found in Supporting Information.

Adsorbate	Distance to surface (Å)	ΔG_{AMOEBA} (1D)	Distance to surface (Å)	$\Delta G_{RigidIon}$ (1D)
$Ca^{2+(64)}$	3.1	-8.5	3.6	+27.3
$CO_3^{2-(64)}$	3.3	+7.0	HL1 2.7/ HL2 3.5	+3.5/-2.5
Acetate	3.1	+4.8	3.6	+31.7
Gly C-terminus	3.2	-1.4	3.0	+51.4
Gly N-terminus	3.4	-4.7	3.3	+9.3
Methylammonium	3.6	-4.6	3.3	+7.1

Table 2. Adsorption free energies (kJ/mol) of acetate, glycine, methylammonium, carbonate and calcium on the obtuse and acute steps of the $\{10\bar{1}4\}$ calcite surface relative to bulk solution. Distances between the adsorbing species and the surface (heights) are given relative to the upper layer of calcium ions. Only the main energy minima from the 1D profiles are reported. The full list of all minima both from 1D profiles and from the minimum energy paths of the 2D profiles can be found in Supporting Information.

Adsorbate	Site	Height (Å)	ΔG_{AMOEBA}	$\Delta G_{RigidIon}$	Site	Height (Å)	ΔG_{AMOEBA}	$\Delta G_{RigidIon}$
Ca^{2+}	Obtuse A	-0.1	+1.2	+44.5, +25.9[34]	Acute A	0.0	-13.8	+15.9, +5.5[34]
		2.9	-0.3	+11.5, +3.5[34]		2.0	-11.0	+12.5, +6.8[34]
	Obtuse B	0.0	+2.4	+43.3, +37.5[34]	Acute B	0.0	+4.7	+23.8, +42.0[34]
		2.5	-3.2	+15.5, +7.0[34]		2.1	+4.4	+17.6, +5.7[34]
		3.1	-1.4	+7.0		3.0	+3.0	+6.3
CO_3^{2-}	Obtuse 1	0.1	+8.6	+9.9, +0.3[34]	Acute 1	0.0	+7.8	-0.5, -10.0[34]
		2.1	-20.5	-9.0, -12.6[34]		2.5	+7.2	-20.8, -20.2[34]
	Obtuse 2	0.0	+26.8	+7.6, +9.5[34]	Acute 2	0.2	+19.7	+5.5, +12.2[34]
		2.7	-10.5	-7.3, -7.7[34]		2.2	No min	-6.4, -7.5[34]
Acetate	Obtuse 1	0.2	+17.9	+55.6	Acute 1	0.0	+8.0	+28.1
		2.1	+3.4	+14.8	(3CV)	2.8	-2.9	+7.3
	Obtuse 2	0.0	+13.8	+57.5	Acute 2	0.3	+15.4	+64.3
		2.7	-8.5	No min		3.3	+7.4	No min
Gly C-ter	Obtuse 1	0.1	+12.0	+62.8	Acute 1	0.0	-2.1	+81.1
		1.5	+6.2	No min	3CV	1.7	-0.1	No min
	Obtuse 2	0.0	+9.7	No min		3.1	+0.3	No min
		2.8	-10.4	No min	Acute 2	0.2	+7.3	+69.7
Gly N-ter	Obtuse A	0.6	+0.6	+20.8	Acute A	0.4	-13.0	No min
		2.1	+5.7	No min		2.1	-3.8	No min
		3.5	-2.6	+4.3		3.2	-4.0	+8.5
	Obtuse B	0.5	+3.9	+24.0	Acute B	0.5	+1.8	No min
		3.4	-2.4	+6.2		3.4	-3.4	No min
$CH_3NH_3^+$	Obtuse A	0.5	+3.3	+18.5	Acute A	0.4	-0.5	No min
		2.4	+3.1	No min		2.3	-0.5	No min
		3.4	-3.0	+5.4		3.4	-4.0	+5.6
	Obtuse B	0.4	+6.6	+25.2	Acute B	0.5	+8.7	No min
		3.3	-1.0	+7.4		3.4	-2.4	No min

TOC image